Steel and Composite Structures, *Vol. 35, No. 1* (*2020*) *29-41*
DOI: https://doi.org/10.12989/scs.2020.35.1.029

Analysis of rotational end restraint for cross-beams of railway through truss bridges

Wojciech Siekierski*

Poznań University of Technology, Institute of Civil Engineering
ul. Piotrowo 5, 61-138 Poznań, Poland

(*Received July 19, 2019, Revised February 12, 2020, Accepted March 5, 2020*)

Abstract. Cross-beams of modern through truss bridges are connected to truss chord at its nodes and between them. It results in variable rotational end restraint for cross-beams, thus variable bending moment distribution. This feature is captured in three-dimensional modelling of through truss bridge structure. However, for preliminary design or rapid assessment of service load effects such technique of analysis may not be available. So an analytical method of assessment of rotational end restraint for cross-beam of through truss bridges was worked out. Two cases – nodal cross-beam and inter-nodal cross-beam – were analyzed. Flexural and torsional stiffness of truss members, flexural stiffness of deck members and axial stiffness of wind bracing members in the vicinity of the analyzed cross-beam were taken into account. The provision for reduced stiffness of the X-type wind bracing was made. Finally, general formula for assessment of rotational end restraint was given. Rotational end restraints for cross-beams of three railway through truss bridges were assessed basing on the analytical method and the finite element method (three-dimensional beam-element modelling). Results of both methods show good agreement. The analytical method is able to reflect effects of some structural irregularities. On the basis of the obtained results the general values of rotational end restraint for nodal and inter-nodal cross-beams of railway through truss bridges were suggested.

Keywords: rotational end restraint; cross-beam; through truss bridge

1. Introduction

Despite advanced techniques of structural analysis, ie. analysis of a complete structure by means of the finite element method (FEM), there is still interest in the analysis of separate structural members accounting for their true restraints. Member stability under compression has been researched for the longest period of time. Partial rotational and torsional fixity at the tips of columns and arches is still investigated. The analysis of influence of torsional end restraint provided by haunched steel girders (Blum and Rasmussen 2018) and the analysis of influence of rotational end restraint (Adman and Saidani 2013, Wangbao and Lizhong 2016) on stability of columns were carried out. In the case of arches the influence of rotational end restraint on global in-plane stability and/or lateral-torsional buckling of steel circular arches (Yan *et al*. 2017), thin-walled arches (Pi and Bradford 2013a) and shallow arches (Pi and Bradford 2013 b,c) was analysed. Issues of end restraint at the tips of columns and girders are also involved in the analysis of fire resistance (Wu and Zhang 2017) and vibrations (Nguyena and Kim 2017) of structural members and assemblies. The restraint provided by girder structural arrangement is also considered in the analysis of local stability in the vicinity of intermediate supports (Wangbao *et al.* 2015, Wangbao *et al.* 2016) and web openings (Durif *et al.* 2015). Another investigated problem is lateral torsional buckling of purlins restrained at their top by roof panels. Research papers on the influence of sandwich panels (Balázs *et al.* 2016, Balázs and Melcher 2017), metal panels (Gao and Moen 2012) and sheet-to-purlin fasteners arrangement (Gajdzicki 2018) can be found. The influence of horizontal lateral restraints is also analysed as a factor of development of catenary action of multi-span girders in RC frames (Lim *et al*. 2017). The aforementioned phenomena are investigated by means of experiment, analysis of structural mechanics or the FEM.

Fig. 1 Location of cross-beams in a modern through truss bridge

*Corresponding author, Ph.D.
E-mail: Wojciech.Siekierski@put.poznan.pl

ISSN: 1229-9367 (Print), 1598-6233 (Online)

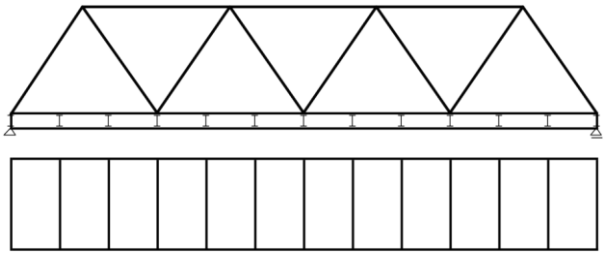

Fig. 2 Layout of through truss bridge with rigid lower chord: longitudinal section (top), plan (bottom)

In the case of cross-beams of through truss bridges rotational end restraint varies from beam to beam. It is so because each of them is attached to the truss node of different stiffness characteristics due to variable truss member cross- sections along the truss span. Moreover some of cross-beams of modern through truss bridges are connected directly to the truss girder nodes (no.1 in Fig. 1) while others are connected to truss chord away from the truss girder nodes (no.2 in Fig. 1) – the example layout is shown in Fig. 2. So the scatter of the magnitude of rotational end restraint is even more substantial.

The analysis of cross-beams of such structures is usually based on numerical analysis, mainly computer-oriented finite element method (FEM). Cross-beams of modern through truss bridges are usually analysed as a part of 3D beam-element models for the purpose of general analysis (Caglayan *et al.* 2012, Cavadas *et al.* 2013) and shell-element models for the purpose of joint analysis (Vičan *et al.* 2014, Wang *et al.* 2009). The former allow for the assessment of bending moment distribution along cross-beams while the latter allow for the assessment of stress distribution within their connections to truss girders. However, sometimes the assessment of bending moment distribution along a cross-beam has to be carried out without global computational model. One of the examples is preliminary design of cross-beams and the other – need for rapid assessment of service load effects. In both cases the accuracy of results can be improved by taking into account cross-beam rotational end restraint instead of analysing the beam as simply supported one.

Rotational end restraint for a cross-beam, that governs bending moment distribution, depends on flexural and torsional stiffness of truss and deck members as well as axial stiffness of wind bracing. It usually differs from cross-beam to cross-beam not only because truss member stiffness vary alongside the span but also because some cross-beams are connected to chord nodes while others – to the chord between the nodes. Fig. 2 shows that there are, in general, three types on cross-beams in terms of rotational end restraint:

a) support cross-beams (the outermost cross-beam over bearings) – rotational end restraint is influenced by bearing type – old-type steel bearings that allow rotation in the girder plane only versus modern bearings allowing multi-axial rotation,
b) nodal cross-beams (connected to chord nodes) – rotational end restraint is influenced mostly by flexural and torsional stiffness of truss diagonals,
c) inter-nodal cross-beams (connected to the chord between the nodes) – rotational end restraint is influenced mostly by torsional stiffness of truss chord.

The paper presents analytical method for setting rotational end restraint for a cross-beam in order to analyze it as a separate member. It is aimed at preliminary design and rapid assessment of bending moment distribution caused by service loads.

2. Analysis of cross-beam rotational end restraint

2.1 Assumptions

For the purpose of further analysis the following assumptions are made:

1. Cross-beam cross-section does not change over its length – it is common in through truss bridges.
2. Truss girders of the analysed bridge span have "W" diagonals pattern (Warren truss) – such diagonals arrangement is usually applied in modern truss bridges.
3. Truss lower chord members and cross-beams axes intersect with no eccentricities – influence of axial forces in cross-beams on moment equilibrium equation at the nodes is small.
4. Bottom wind bracing axes may be offset from cross-beams axes (eccentricity) – location of wind bracing out of neutral plane of cross-beams is common for bridges.
5. Cross-beam – to – truss chord connection is undeformable – bridge structures usually have rigid connections; pinned connection implies a simply supported cross-beam.
6. Truss diagonals are clamped at the nodes of truss upper chord in terms of torsion – existence of separate or integrated gusset plates at the truss nodes is assumed to imply such restraint.
7. Within the analysed part of the structure the gradient of linear displacement of adjacent nodes is small and thus has limited influence on bending moments in truss members – the nodes where cross-beams are connected to lower chord as well as nodes where diagonals are connected to upper chord are assumed to be pin-supported.
8. Rotational end restraint of a cross-beam at its connection to truss chord depends on stiffness of the nearest chord members, truss diagonals, cross-beams and wind bracing members – assumed for the sake of practical applicability of the analytical method.
9. Strains are small and steel stays within elastic range – justified for the analysis of service load effects.
10. Track axis coincides with structural symmetry axis – it is common for single track railway bridges.

2.2 Notation

Global and local axes are explained in Fig. 3. Truss girder is assumed to be situated in the plane parallel to the XOZ plane. Local x axis of truss diagonals is the member

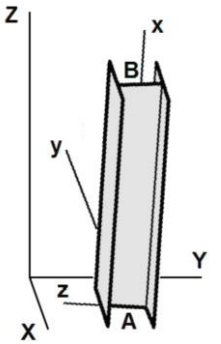

Fig. 3 Global (X, Y, Z) and local (x, y, z) axes

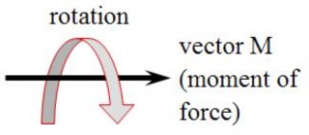

Fig. 4 Explanation of vector M

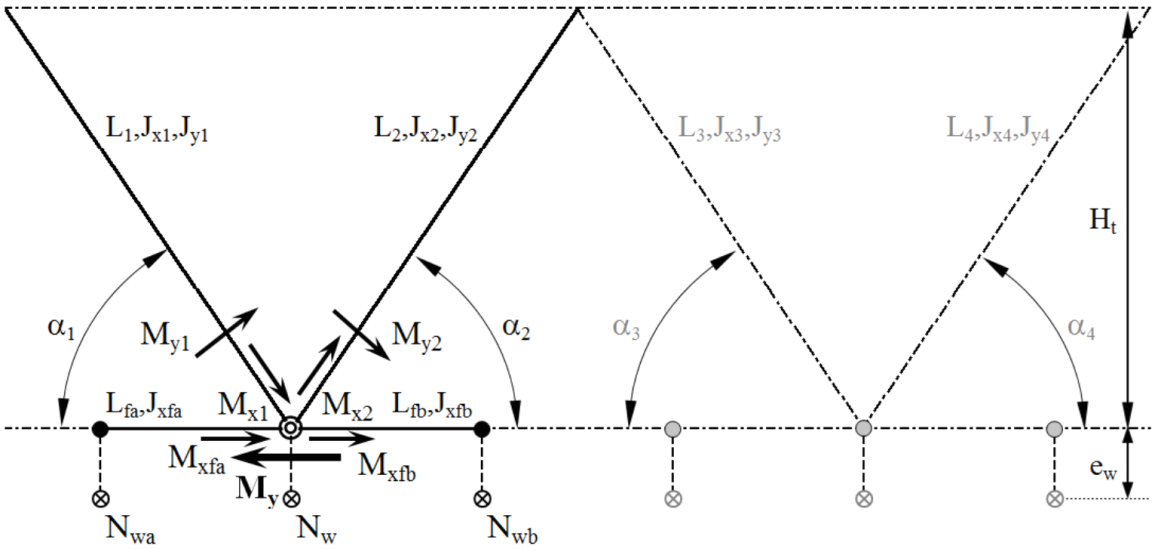

Fig. 5 Analysis of rotational end restraint for nodal cross-beam (the analysed cross-beam marked by double circle, "active" members marked by continuous lines, dark dots and dark crossed circles)

longitudinal axis, local y axis of diagonals is in the truss girder plane. Local z axis of diagonals is orthogonal to the truss girder plane. Local x axis of chord members, cross-beams and wind bracing members is as for diagonals. Local z axis of all the members is vertical. Their local y axis is set according to the right-hand rule. Moment vector direction is explained in Fig. 4.

2.3 Support cross-beams

The rotational end restraint for cross-beam is suggested to be assumed as:

– infinity (clamping) – in the case of "old-fashioned" curved-cylindrical or roller steel bearings that allow rotation only around the horizontal axis perpendicular to span,
– partial fixity (flexible) – in the case of modern pot bearings and spherical bearings that allow rotation around any horizontal axis (for details see the chapter 2.4).

2.4 Nodal cross-beams

It is assumed that the end rotation of a cross-beam connected to a truss lower chord node is restrained by the structural system consisted of: the adjacent diagonals, the adjacent chord members, the adjacent cross-beams and the respective members of bottom wind bracing – marked in Fig. 5.

At the node where the analysed cross-beam is connected to the truss chord there is equilibrium of moments

(projection of vectors of moments on the axis of lower chord)

$$M_y = M_{x1} \cdot cos\alpha_1 + M_{x2} \cdot cos\alpha_2 + M_{y1} \cdot sin\alpha_1 + \\ + M_{y2} \cdot sin\alpha_2 + N_w \cdot cos\omega \cdot e_w + M_{xfa} + M_{xfb} \quad (1)$$

M_y – the bending moment in the analyzed cross-beam at its connection to truss chord, kNm,
M_{xi} – the torsional moment near the analyzed cross-beam in the i-th diagonal, kNm,
M_{yi} – the bending moment near the analyzed cross-beam in the i-th diagonal, kNm,
N_w – the axial force in the wind bracing member connected to the node with the analyzed cross-beam, kN,
M_{xfa}, M_{xfb} – the torsional moment in the lower chord member to the left ("a") and right ("b") of the node where the analyzed cross-beam is connected, respectively, kNm,
α_i – the angle of inclination of the i-th diagonal in the reference to the lower chord, rad,
ω – the angle (in the horizontal plane) between the wind bracing member and the cross-beam meeting the chord at the same joint, rad,
e_w – the eccentricity of the wind bracing member in respect to the cross-beam centre of gravity, m.

At the connections of the adjacent cross-beams to the truss chord the following states of equilibrium of moments occur:
– at the connection on the left

$$M_{xfa} = M_{yca} + N_{wa} \cdot cos\omega \cdot e_w \quad (2)$$

– at the connection on the right:

$$M_{xfb} = M_{ycb} + N_{wb} \cdot cos\omega \cdot e_w \quad (3)$$

where
M_{yca}, M_{ycb} – the bending moment in the cross-beam to the left ("a") and right ("b") of the analyzed one, respectively, kNm,
N_{wa}, N_{wb} – the axial force in the wind bracing member connected to the node to the left ("a") and right ("b") of the node with the analyzed cross-beam, respectively, kN.

The moments given on the right side of Eq. (1) are coupled with the respective member end rotations and elongations as follows:
– for torsion of the i-th diagonal (i=1, 2)

$$\frac{\varphi_i}{L_i} \cdot GJ_{xi} = M_{xi} \quad (4)$$

– for flexure of the i-th diagonal (i=1, 2)

$$\frac{k \cdot \gamma_i}{L_i} \cdot EJ_{yi} = M_{yi} \quad (5)$$

– for the truss chord members to the left ("a") and right ("b") of the analysed cross-beam

$$\frac{\varphi_a}{L_{fa}} \cdot GJ_{fxa} = M_{xfa} \quad \text{and} \quad \frac{\varphi_b}{L_{fb}} \cdot GJ_{fxb} = M_{xfb} \quad (6)$$

– for any member of bottom wind bracing connected to the same node as the analyzed cross-beam

$$\frac{\Delta L_w}{L_w} \cdot EA_w = N_w \quad (7)$$

where:
E – the modulus of elasticity for steel, kPa,
G – the shear modulus for steel, kPa,
φ_i – the angle of torsion of the i-th diagonal, rad.
γ_i – the angle of rotation out of the truss plane of the i-th diagonal due to bending, rad,
J_{xfa}, J_{xfb} – moment of inertia in torsion for the chord member to the left ("a") and right ("b") of the node with the analyzed cross-beam, up to the nearest cross-beam connection, m^4,
J_{xi} – the moment of inertia in torsion for the i-th diagonal, m^4,
J_{yi} – the moment of inertia in bending for the i-th diagonal, m^4,
A_w – the cross-sectional area of the wind bracing member connected to the analyzed cross-beam at the truss chord, m^2,
L_{fa}, L_{fb} – the length of the chord member between the connection of the analyzed cross-beam and connection of the cross-beam to the left ("a") and right ("b") of the analyzed one, respectively, m,
L_i – the theoretical length of the i-th diagonal, m,
L_w – the length of the wind bracing member connected, at the truss chord, to the analyzed cross-beam, measured up to the plane of longitudinal symmetry of the span, m
k – the coefficient dependent on truss diagonal rotational constraints (out of the truss plane) at upper chord: k=3 – for an open-section upper chord and/or weak/absent bracing in the plane of top chords of truss girders (pinned connection), k=4 – for a closed-section upper chord and/or heavy bracing in the plane of top chords of truss girders (clamped connection).

Due to bending of the analyzed cross-beam the node where it is connected to the truss chord rotates by the angle β. Transformation of β to the rotations of the diagonals and elongation of the wind bracing member is as follows

$$\varphi_i = \beta \cdot cos\alpha_i \quad (8)$$

$$\gamma_i = \beta \cdot sin\alpha_i \quad (9)$$

$$\Delta L_w = \frac{\beta \cdot e_w}{cos\omega} \quad (10)$$

where:
β – the angle of end rotation of the end of the analyzed cross-beam (due to M_y), rad.

Since the part of the structure marked by continuous lines in Fig. 5 is assumed to be isolated from the rest the equilibrium of angles of rotation/torsion occurs

$$\beta = \beta_a + \varphi_a \quad \text{and} \quad \beta = \beta_b + \varphi_b \quad (11)$$

where:
β_a, β_b – the angles of rotation of the end of the cross-beams to the left (the index "a") and right (the index "b") of the analyzed one, rad,

φ_a, φ_b – the angles of torsion of the lower chord between the analyzed cross-beam and the cross-beams to the left ("a") and right ("b") of it, rad.

Substituting Eqs. (8)-(10) into Eqs. (4), (5), (7) the following is obtained

$$\frac{\beta \cdot cos\alpha_i}{L_i} \cdot GJ_{xi} = M_{xi} \tag{12}$$

$$\frac{k \cdot \beta \cdot sin\alpha_i}{L_i} \cdot EJ_{yi} = M_{yi} \tag{13}$$

$$\frac{\beta \cdot e_w}{L_w \cdot cos\omega} \cdot EA_w = N_w \tag{14}$$

The rotations β_a and β_b at the nodes where the cross-beams to the left and right of the analysed one are connected to the truss chord generate the following internal forces:

– bending of the cross-beams to the left ("a") and right ("b") of the analyzed one

$$\frac{4 \cdot \beta_a}{L_{ca}} \cdot EJ_{yca} = M_{yca} \quad \text{and} \quad \frac{4 \cdot \beta_b}{L_{cb}} \cdot EJ_{ycb} = M_{ycb} \tag{15}$$

– tension in the bottom wind bracing members connected to the nodes to the left ("a") and right ("b") of the one where the analyzed cross-beam is connected

$$\frac{\beta_a \cdot e_w}{L_{wa} \cdot cos\omega} \cdot EA_{wa} = N_{wa} \quad \text{and} \quad \frac{\beta_b \cdot e_w}{L_{wb} \cdot cos\omega} \cdot EA_{wb} = N_{wb} \tag{16}$$

where

J_{yca}, J_{ycb} – the moment of inertia in bending for the cross-beam to the left ("a") and right ("b") of the analyzed one, m^4,

L_{ca}, L_{cb} – the theoretical length of the cross-beam to the left ("a") and right ("b") of the analyzed one, m,

L_{wa}, L_{wb} – the length of the wind bracing member connected, at the truss chord, to the cross-beam to the left ("a") and right ("b") of the analyzed one, measured up to the plane of longitudinal symmetry of the span, m.

So Eqs. (2) and (3) may be written as

$$M_{xfa} = \frac{4 \cdot \beta_a}{L_{ca}} \cdot EJ_{yca} + \frac{\beta_a \cdot e_w^{\,2}}{L_{wa}} \cdot EA_{wa} \tag{17}$$

$$M_{xfb} = \frac{4 \cdot \beta_b}{L_{cb}} \cdot EJ_{yca} + \frac{\beta_b \cdot e_w^{\,2}}{L_{wb} \cdot cos\omega} \cdot EA_{wb} \tag{18}$$

Thus

$$\beta_a = \frac{M_{xfa}}{\frac{4}{L_{ca}} \cdot EJ_{yca} + \frac{e_w^{\,2}}{L_{wa}} \cdot EA_{wa}} \tag{19}$$

$$\beta_b = \frac{M_{xfb}}{\frac{4}{L_{cb}} \cdot EJ_{yca} + \frac{e_w^{\,2}}{L_{wb}} \cdot EA_{wb}} \tag{20}$$

Rewriting Eq. (6) to obtain φ and substituting this and Eqs. (19) and (20) to Eq. (11) we obtain

$$\beta = \beta_a + \varphi_a = \frac{M_{xfa}}{\frac{4}{L_{ca}} \cdot EJ_{yca} + \frac{e_w^{\,2}}{L_{wa}} \cdot EA_{wa}} + \frac{M_{xfa}}{\frac{1}{L_{fa}} \cdot GJ_{fxa}} \tag{21}$$

$$\beta = \beta_b + \varphi_b = \frac{M_{xfb}}{\frac{4}{L_{cb}} \cdot EJ_{ycb} + \frac{e_w^{\,2}}{L_{wb}} \cdot EA_{wb}} + \frac{M_{xfb}}{\frac{1}{L_{fb}} \cdot GJ_{fxb}} \tag{22}$$

Hence

$$M_{xfa} = \frac{\beta}{\frac{1}{\frac{4}{L_{ca}} \cdot EJ_{yca} + \frac{e_w^{\,2}}{L_{wa}} \cdot EA_{wa}} + \frac{1}{\frac{1}{L_{fa}} \cdot GJ_{fxa}}} \tag{23}$$

$$M_{xfb} = \frac{\beta}{\frac{1}{\frac{4}{L_{cb}} \cdot EJ_{ycb} + \frac{e_w^{\,2}}{L_{wb}} \cdot EA_{wb}} + \frac{1}{\frac{1}{L_{fb}} \cdot GJ_{fxb}}} \tag{24}$$

Substituting Eqs. (12)-(14), (23) and (24) to Eq. (1) and dividing both sides by β the rotational end restraint r_c for the analysed cross-beam is obtained as follows

$$\begin{aligned} r_c = \frac{M_y}{\beta} = &\sum_{i=1}^{2}\left(\frac{cos\alpha_i}{L_i} \cdot GJ_{xi} + \frac{k \cdot sin\alpha_i}{L_i} \cdot EJ_{yi}\right) + \\ &+ \frac{e_w^{\,2}}{L_w} \cdot EA_w + \\ &+ \frac{1}{\frac{1}{\frac{4}{L_{ca}} \cdot EJ_{yca} + \frac{e_w^{\,2}}{L_{wa}} \cdot EA_{wa}} + \frac{1}{\frac{1}{L_{fa}} \cdot GJ_{fxa}}} + \\ &+ \frac{1}{\frac{1}{\frac{4}{L_{cb}} \cdot EJ_{ycb} + \frac{e_w^{\,2}}{L_{wb}} \cdot EA_{wb}} + \frac{1}{\frac{1}{L_{fb}} \cdot GJ_{fxb}}} \end{aligned} \tag{25}$$

Under the assumption that the truss girder is regular, i.e.: $\alpha_i = L_i = const$ (the index "i" may be omitted) and $L_{ca} = L_{cb} = L_c$, $L_{wa} = L_{wb} = L_w$, the following is obtained

$$\begin{aligned} r_c = \frac{M_y}{\beta} = &\frac{cos\alpha}{L} \cdot G\left(J_{x1} + J_{x2}\right) + \\ &+ \frac{k \cdot sin\alpha}{L} \cdot E\left(J_{y1} + J_{y2}\right) + \frac{e_w^{\,2}}{L_w} \cdot EA_w + \\ &+ \frac{1}{\frac{1}{\frac{4}{L_c} \cdot EJ_{yca} + \frac{e_w^{\,2}}{L_w} \cdot EA_{wa}} + \frac{1}{\frac{1}{L_f} \cdot GJ_{fxa}}} + \\ &+ \frac{1}{\frac{1}{\frac{4}{L_c} \cdot EJ_{ycb} + \frac{e_w^{\,2}}{L_w} \cdot EA_{wb}} + \frac{1}{\frac{1}{L_f} \cdot GJ_{fxb}}} \end{aligned} \tag{26}$$

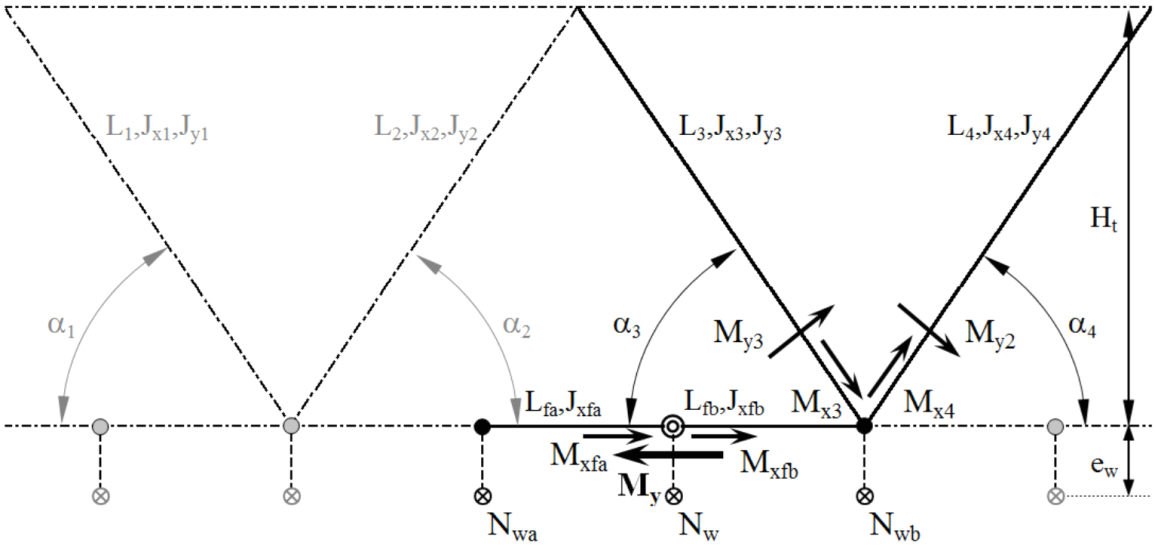

Fig. 6 Analysis of rotational end restraint for inter-nodal cross-beam (the analysed cross-beam marked by double circle, "active" members marked by continuous lines, dark dots and dark crossed circles)

2.5 Inter-nodal cross-beams

It is assumed that end rotation of a cross-beam connected to the truss lower chord between nodes is restrained by the structural system consisted of: the adjacent chord members, the adjacent cross-beams, the adjacent diagonals (if any) and the respective members of bottom wind bracing – marked in Fig. 6.

At the node where the analysed cross-beam is connected to the truss chord there is equilibrium of moments (projection of vectors of moments on the axis of the lower chord)

$$M_y = M_{xfa} + M_{xfb} + N_w \cdot cos\omega \cdot e_w \tag{27}$$

The two torques on the right side of Eq. (27) are coupled with member end rotations according to the following

$$\frac{\varphi_{fa}}{L_{fa}} \cdot GJ_{xfa} = M_{xfa} \tag{28}$$

$$\frac{\varphi_{fb}}{L_{fb}} \cdot GJ_{xfb} = M_{xfb} \tag{29}$$

At the truss chord connections to the cross-beams adjacent to the one with the analyzed cross-beam the equilibrium of moments is (respectively):
– at the connection on the left

$$M_{xfa} = M_{yca} + N_{wa} \cdot cos\omega \cdot e_w \tag{30}$$

– at the connection on the right:

$$\begin{aligned} M_{xfb} &= M_{x3} \cdot cos\alpha_3 + M_{x4} \cdot cos\alpha_4 + \\ &+ M_{y3} \cdot sin\alpha_3 + M_{y4} \cdot sin\alpha_4 + \\ &+ M_{ycb} + N_{wb} \cdot cos\omega \cdot e_w \end{aligned} \tag{31}$$

The part of the structure marked by continuous lines if Fig. 6 is assumed to be isolated from the rest. Thus the equilibrium of the angles of rotation/torsion given in Eq. (11) is valid.

The moments given on the right side of Eqs. (30) and (31) are coupled with the respective member end rotations and elongations and can be described as in Eqs. (4)-(7), (15) and (16). So the two torques on the left side of Eqs. (31) and (31) can be expressed as

$$M_{xfa} = \frac{4 \cdot \beta_a}{L_{ca}} \cdot EJ_{yca} + \frac{\beta_a \cdot e_w^{\,2}}{L_{wa}} \cdot EA_{wa} \tag{32}$$

$$\begin{aligned} M_{xfb} = &\sum_{i=3}^{4} \left(\frac{\beta_b \cdot cos\alpha_i}{L_i} \cdot GJ_{xi} + \frac{k \cdot \beta_b \cdot sin\alpha_i}{L_i} \cdot EJ_{yi} \right) + \\ &+ \frac{4 \cdot \beta_b}{L_{cb}} \cdot EJ_{yca} + \frac{\beta_b \cdot e_w^{\,2}}{L_{wb}} \cdot EA_{wb} \end{aligned} \tag{33}$$

So the angles β_a and β_b are equal:

$$\beta_a = \frac{M_{xfa}}{\frac{4}{L_{ca}} \cdot EJ_{yca} + \frac{e_w^{\,2}}{L_{wa}} \cdot EA_{wa}} \tag{34}$$

$$\beta_b = \frac{M_{xfb}}{\left[\sum_{i=3}^{4} \left(\frac{cos\alpha_i}{L_i} \cdot GJ_{xi} + \frac{k \cdot sin\alpha_i}{L_i} \cdot EJ_{yi} \right) + \right.} \left. + \frac{4}{L_{cb}} \cdot EJ_{yca} + \frac{e_w^{\,2}}{L_{wb}} \cdot EA_{wb} \right] \tag{35}$$

Based on Eq. (11), using Eqs. (6), (34) and (35) the following is obtained

$$\beta = \beta_a + \varphi_{fa} = \\ = M_{xfa} \cdot \left(\frac{1}{\frac{4}{L_{ca}} \cdot EJ_{yca} + \frac{e_w^{\,2}}{L_{wa}} \cdot EA_{wa}} + \frac{L_{fa}}{GJ_{xfa}} \right) \tag{36}$$

$$\beta = \beta_b + \varphi_{fb} = \\ = M_{xfb} \cdot \left\{ \begin{array}{l} \dfrac{1}{\left[\sum\limits_{i=3}^{4} \left(\dfrac{\cos\alpha_i}{L_i} \cdot GJ_{xi} + \dfrac{k \cdot \sin\alpha_i}{L_i} \cdot EJ_{yi} \right) + \right.} + \\ \left. + \dfrac{4}{L_{cb}} \cdot EJ_{ycb} + \dfrac{e_w^{\,2}}{L_{wb}} \cdot EA_{wb} \right] \\ + \dfrac{L_{fb}}{GJ_{xfb}} \end{array} \right\} \tag{37}$$

So the torques M_{xfa} and M_{xfb} are

$$M_{xfa} = \frac{\beta}{\frac{1}{\frac{4}{L_{ca}} \cdot EJ_{yca} + \frac{e_w^{\,2}}{L_{wa}} \cdot EA_{wa}} + \frac{L_{fa}}{GJ_{xfa}}} \tag{38}$$

$$M_{xfb} = \frac{\beta}{\left\{ \begin{array}{l} \dfrac{1}{\left[\sum\limits_{i=3}^{4} \left(\dfrac{\cos\alpha_i}{L_i} \cdot GJ_{xi} + \dfrac{k \cdot \sin\alpha_i}{L_i} \cdot EJ_{yi} \right) + \right.} + \\ \left. + \dfrac{4}{L_{cb}} \cdot EJ_{ycb} + \dfrac{e_w^{\,2}}{L_{wb}} \cdot EA_{wb} \right] \\ + \dfrac{L_{fb}}{GJ_{xfb}} \end{array} \right\}} \tag{39}$$

Substituting in Eq. (27) for the internal forces on the right side and dividing by β, the rotational end restraint for the analysed cross-beam is given as

$$r_c = \frac{M_y}{\beta} = \frac{1}{\frac{1}{\frac{4}{L_{ca}} \cdot EJ_{yca} + \frac{e_w^{\,2}}{L_{wa}} \cdot EA_{wa}} + \frac{L_{fa}}{GJ_{xfa}}} + \\ + \frac{1}{\left\{ \begin{array}{l} \dfrac{1}{\left[\sum\limits_{i=3}^{4} \left(\dfrac{\cos\alpha_i}{L_i} \cdot GJ_{xi} + \dfrac{k \cdot \sin\alpha_i}{L_i} \cdot EJ_{yi} \right) + \right.} + \\ \left. + \dfrac{4}{L_{cb}} \cdot EJ_{ycb} + \dfrac{e_w^{\,2}}{L_{wb}} \cdot EA_{wb} \right] \\ + \dfrac{L_{fb}}{GJ_{xfb}} \end{array} \right\}} + \\ + \frac{e_w^{\,2}}{L_w} \cdot EA_w \tag{40}$$

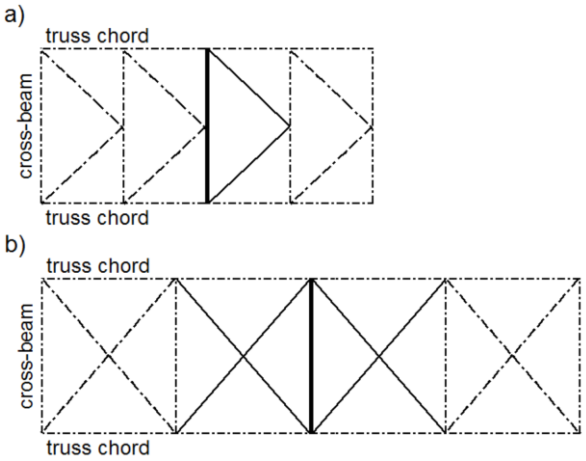

Fig. 7 Wind bracing layouts: (a) K-type, (b) X-type (the analyzed cross-beam marked with thick line, "active" wind bracing marked with continuous lines)

Under the assumption that the truss girder is regular, i.e.: $\alpha_i = L_i = \text{const}$ (the index "i" may be omitted) and $L_{ca} = L_{cb} = L_c$, $L_{wa} = L_{wb} = L_w$, the following is obtained

$$r_c = \frac{M_y}{\beta} = \frac{1}{\frac{1}{\frac{4}{L_c} \cdot EJ_{yca} + \frac{e_w^{\,2}}{L_w} \cdot EA_{wa}} + \frac{L_f}{GJ_{xfa}}} + \\ + \frac{1}{\left\{ \begin{array}{l} \dfrac{1}{\left[\dfrac{\cos\alpha}{L} \cdot G(J_{x3} + J_{x4}) + \right.} + \\ + \dfrac{k \cdot \sin\alpha}{L} \cdot E(J_{y3} + J_{y4}) + \\ \left. + \dfrac{4}{L_c} \cdot EJ_{ycb} + \dfrac{e_w^{\,2}}{L_w} \cdot EA_{wb} \right] \\ + \dfrac{L_f}{GJ_{xfb}} \end{array} \right\}} + \\ + \frac{e_w^{\,2}}{L_w} \cdot EA_w \tag{41}$$

2.6 Restraint provided by X-type wind bracing

The analysis presented above assumes that joint action of a cross-beam and the respective wind bracing members is independent from the adjacent cross-beam behaviour. It is valid for the K-type wind bracing (Fig. 7(a)) where each bracing leg is situated between the end of the analyzed cross-beam and the centre point of the adjacent one. It is justified to assume that the point does not change position due to substantial out-of-plane stiffness of the adjacent cross-beam. In this case elongation of the analyzed cross-beam (thick line) bottom fibre due to bending activates the

nearest wind bracing legs (continuous line) and the restraint provided by wind bracing is based on its appropriate stiffness and the assumed length. In the case of the X-type wind bracing (Fig. 7(b)) two adjacent sections of bracing (continuous line) respond to bending of the analyzed cross-beam (thick line). The intermediate joint of wind bracing members changes position alongside the span due to unequal flexure of the analysed cross-beam and the adjacent ones. So the restraint provided by the X-type wind bracing to the analyzed cross-beam is smaller than computed on the basis of its appropriate stiffness and assumed length.

To find the reduction coefficient for the X-type wind bracing stiffness four groups of several sets of beam-element computational models of three wind bracing layouts were analyzed. Each group was unique by wind bracing cross-section, i.e.: single and double angle 75×75×8, single and double angle 120×120×12. Each group consisted of 8 model sets, each unique by the ω angle. Each set consisted of three wind bracing layouts: one that assumed zero truss chord axial stiffness (Fig. 8, left), one that assumed infinite truss chord axial stiffness (Fig. 8, middle) and one that represented degenerated X-type wind bracing which intermediate joints cannot change position, acting like double K-type wind bracing (Fig. 8, right). Detailed model characteristics are given in Table 1.

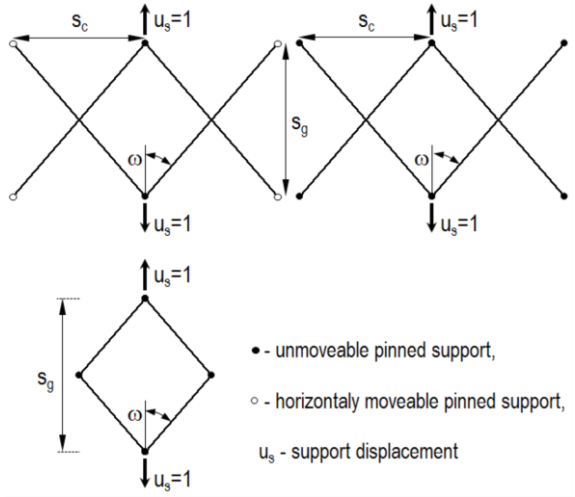

Fig. 8 Set of computational models for the analysis of stiffness of X-type wind bracing

Table 1 Characteristics of the analyzed models of X-type wind bracing layouts

Truss girder spacing s_g [m]	5.5	5.5	5.5	5.5	5.5	5.5	5.5	5.5
Cross beam spacing s_c [m]	2.5	3.0	3.5	4.0	5.5	7.0	8.5	10.0
Angle ω [°]	24.4	28.6	32.5	36.0	45.0	51.8	57.1	61.2

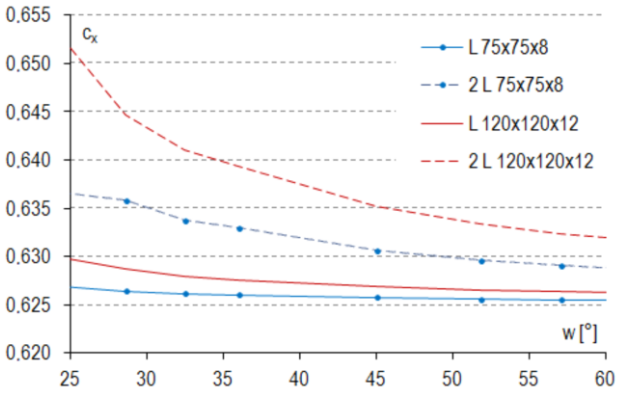

Fig. 9 Variation of reduction coefficient for the stiffness of the X-type wind bracing in reference to the angle between a cross-beam and a leg of wind bracing

For each model in each set the reaction at the displaced support, parallel to displacement direction, was recorded. The reduction coefficient for stiffness of X-type wind bracing was computed as follows

$$c_x = \frac{\frac{1}{2}\cdot\left(R_K + \frac{R_0 + R_\infty}{2}\right)}{R_K} \tag{42}$$

where:

R_0 – the reaction at the support of the model that assumes zero truss chord axial stiffness, kN,

R_∞ – the reaction at the support of the model that assumes infinite truss chord axial stiffness, kN,

R_K – the reaction at the support of the model that represents double K-type wind bracing, kN.

Computation results are presented in diagrams in Fig. 9. It can be seen that for the X-type wind bracing the reduction coefficient for its stiffness, in terms of rotational end restraint provided to cross-beam, may be approximated by 0.630 for single angle bracing at any ω angle, by 0.645 for double angle bracing at ω<45° and 0.635 for double angle bracing at ω≥45°. It should be stressed that for the K-type wind bracing c_x is 1.0 (no reduction).

2.7 General expression for rotational end restraint

Under the assumptions made in the chapter 2.2 the rotational end restraint for any cross-beam at its connection to the truss chord may be expressed as a sum of three components

$$r_c = \frac{M_y}{\beta} = C + A + B \tag{43}$$

where: C – expresses the influence of the joint where the analyzed cross-beam is connected to the truss chord, kNm/rad; A – expresses the influence of the chord member, the cross-beam, the wind bracing members and any truss diagonal directly to the left of the joint, kNm/rad; B – expresses the influence of the chord member, the cross-beam, the wind bracing members and any truss diagonal

directly to the right of the joint, kNm/rad.

Assuming that the truss girder is regular the general formula for the component *C* is

$$C = \frac{\cos\alpha}{L} \cdot G\left(J_{x1} + J_{x2}\right) + \frac{k \cdot \sin\alpha}{L} \cdot E\left(J_{y1} + J_{y2}\right) + \\ + \frac{c_x \cdot e_w^{\,2}}{L_w} \cdot EA_w \tag{44}$$

where all the characteristics refer to the members connected to the joint of the analysed cross-beam and c_x – the reduction coefficient for the X-type wind bracing stiffness.

The general formula for the component *A* is (under assumption that the cross-beam to the left of the analysed one is present)

$$A = \frac{1}{\left\{\begin{array}{l} \dfrac{1}{\left[\begin{array}{l} \dfrac{\cos\alpha}{L} \cdot G(J_{x1a} + J_{x2a}) + \\ + \dfrac{k \cdot \sin\alpha}{L} \cdot E(J_{y1a} + J_{y2a}) + \\ + \dfrac{4}{L_c} \cdot EJ_{yca} + \dfrac{e_w^{\,2}}{L_w} \cdot EA_{wa} \end{array}\right]} + \\ + \dfrac{L_f}{GJ_{xfa}} \end{array}\right\}} \tag{45}$$

where all the characteristics refer to the members connected to the cross-beam to the left of the analysed one.

The general formula for the component *B* is (under assumption that the cross-beam to the right of the analysed one is present)

$$B = \frac{1}{\left\{\begin{array}{l} \dfrac{1}{\left[\begin{array}{l} \dfrac{\cos\alpha}{L} \cdot G(J_{x1b} + J_{x2b}) + \\ + \dfrac{k \cdot \sin\alpha}{L} \cdot E(J_{y1b} + J_{y2b}) + \\ + \dfrac{4}{L_c} \cdot EJ_{ycb} + \dfrac{e_w^{\,2}}{L_w} \cdot EA_{wb} \end{array}\right]} + \\ + \dfrac{L_f}{GJ_{xfb}} \end{array}\right\}} \tag{46}$$

where all the characteristics refer to the members connected to cross-beam to the right of the analysed one.

For all the components (C, A, B) a missing member (a truss diagonal or a wind bracing member) means substitution of "0" for the respective moment of inertia or cross-section area.

3. Validation of the analytical method

To validate the presented analytical method rotational end restraints for cross-beams of three through truss bridge spans (Fig. 10) were computed with an aid of the finite element method and the analytical method presented above.

Structural layouts of truss girders and decks of the three bridge spans are shown in Fig. 11 and their cross-sections – in Fig. 12. All three of them are ballasted track, simply supported span bridges built out of open cross-section members. In each case chord node spacing is a multiple of cross-beam spacing. In the case of the Span-51 and the Span-93 the neutral axis of truss lower chord does not coincide with the chord theoretical axis (see H_t in Fig. 12). Both spans have steel-concrete composite deck and K-type bottom wind bracing. The Span-38 has steel orthotropic deck and X-type bottom wind bracing. The deck slab of the Span-93 has expansion joints at the lower chord nodes – twin cross-beams located there are marked in Fig. 11.

Fig. 10 The analyzed through truss bridge spans: Span-51 (top), Span-93 (middle), Span-38 (bottom)

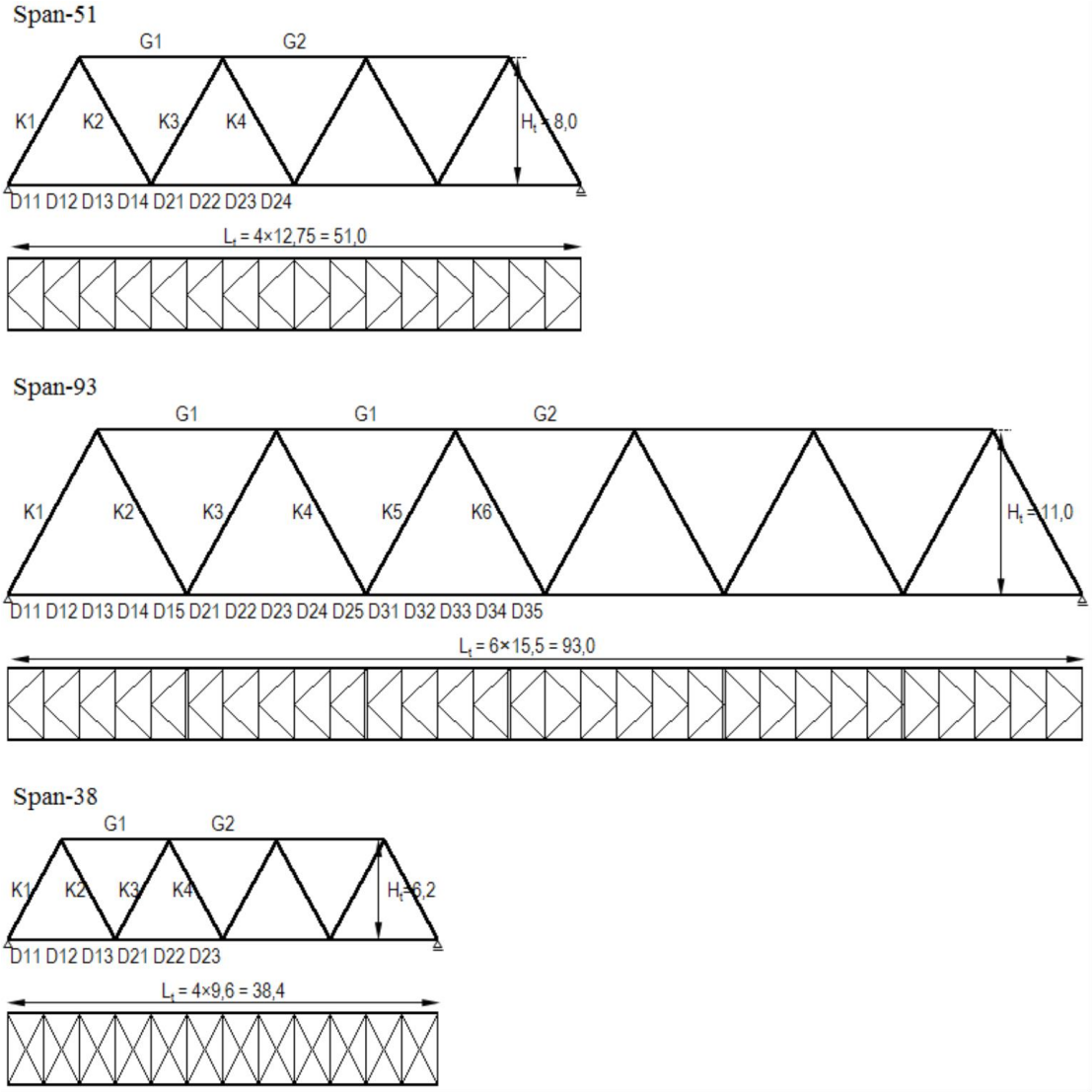

Fig. 11 Layouts of truss girders and decks of the analyzed bridge spans

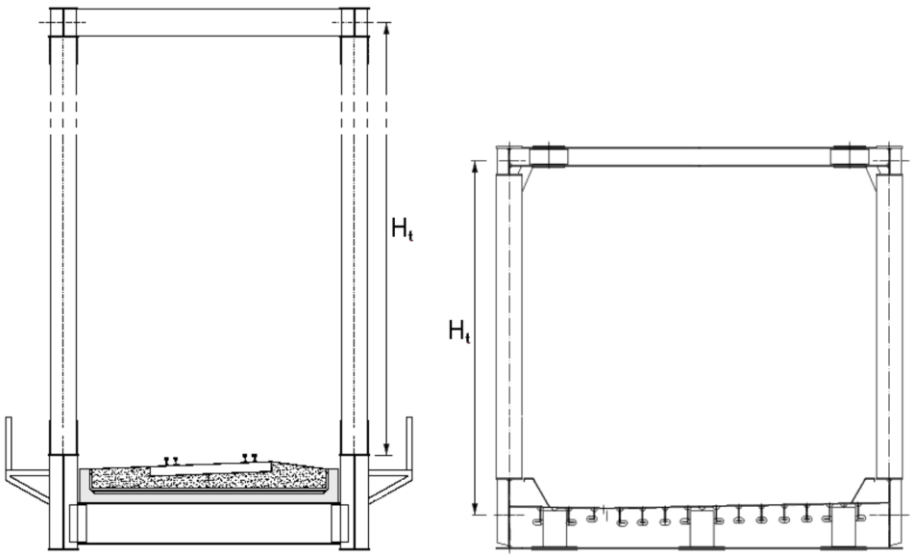

Fig. 12 Bridge span cross-sections: the Span-51 and the Span 93 on the left, the Span-38 on the right

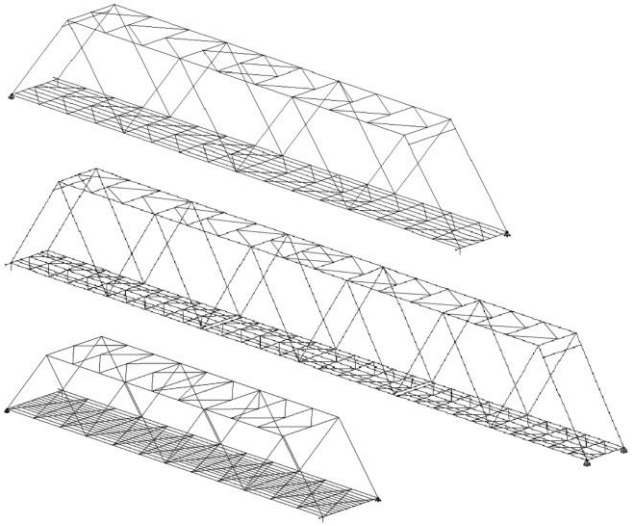

Fig. 13 Finite element models of the Span-51, the Span-93 and the Span-38 respectively (not to scale)

For the analyzed bridge spans three-dimensional numerical models were created in the Autodesk Robot environment (Marsh 2016). The finite element models were created out of beam elements based on structural dimensions and cross-section characteristics found in the design documentation. The models are shown in Fig. 13. Truss girder members, cross-beams and wind bracing members were modelled by 2-node beam elements. The deck slabs were divided into seven (the Span-51) or five (the Span-93) longitudinal strips and modelled also by 2-node beam elements. For the two spans steel-concrete composite action of the cross-beams and the deck slab was taken into account. In the case of the orthotropic deck (the Span-38) each longitudinal rib together with a part of steel plate was modelled by 2-node beam elements. All the computational models accounted for eccentricities of the lower chord members, the cross-beams and the wind bracing members in reference to the chord theoretical nodes. Elastic behaviour and small strains were assumed. Steel properties were taken as: E=205 GPa and G=80.8 GPa. A boogie of ET22 electric locomotive was used as loading – 200 kN per axle and axle spacing: 1.75 m (Fig. 14) Axle loads were modelled in the FE analysis as uniformly distributed loads (thanks to the gravel bed) applied to the respective longitudinal elements modelling the decks. Rotational end restraint was computed as the relationship of the resulted bending moment at the cross-beam connection to the truss chord and the respective rotation of that joint around the chord axis.

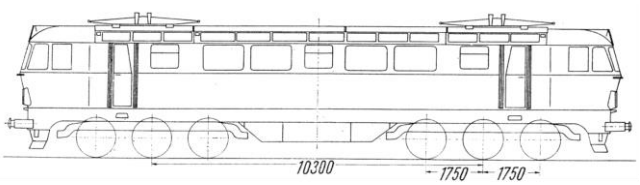

Fig. 14 Scheme of ET 22 electric locomotive (total weight 1200 kN)

Table 2 Characteristics of the analyzed models of X-type wind bracing layouts

	Span-51	Span-93	Span-38
L_t [m]	51.0	93.0	38.4
s_g [m]	5.30	6.00	6.70
e_w [m]	0.65	0.34	0.59
α [°]	51.45	54.83	0.91
J_{xD11} [m^4]	2.313E-06	5.873E-06	4.787E-06
J_{xD12} [m^4]	3.369E-06	3.924E-06	4.787E-06
J_{xD13} [m^4]	3.369E-06	3.924E-06	4.787E-06
J_{xD14} [m^4]	3.369E-06	3.924E-06	-
J_{xD15} [m^4]	-	1.847E-05	-
J_{xD21} [m^4]	7.941E-06	1.847E-05	8.627E-06
J_{xD22} [m^4]	7.941E-06	1.095E-05	8.627E-06
J_{xD23} [m^4]	7.941E-06	1.095E-05	8.627E-06
J_{xD24} [m^4]	7.941E-06	1.095E-05	-
J_{xD25} [m^4]	-	1.095E-05	-
Jx_{D31} [m^4]	-	1.095E-05	-
J_{xD32} [m^4]	-	2.065E-05	-
J_{xD33} [m^4]	-	2.065E-05	-
J_{xD34} [m^4]	-	2.065E-05	-
J_{xD35} [m^4]	-	2.065E-05	-
H_t [m]	8.00	11.00	6.17
s_c [m]	3.19	3.10	3.20
c_x	1	1	0,63
ω [°]	50.26	45.94	0.45
k	3	3	3
J_{yK1} [m4]	8.721E-04	3.190E-03	4.867E-04
J_{yK2} [m4]	5.947E-04	1.679E-03	4.867E-04
J_{yK3} [m4]	4.057E-04	1.852E-03	3.245E-04
J_{yK4} [m4]	2.739E-04	9.904E-04	3.245E-04
J_{yK5} [m4]	-	8.297E-04	-
J_{yK6} [m4]	-	5.244E-04	-
J_{xK1} [m4]	2.432E-06	1.856E-05	8.200E-06
J_{xK2} [m4]	1.100E-06	4.014E-06	8.200E-06
J_{xK3} [m4]	5.753E-07	4.858E-06	2.589E-06
J_{xK4} [m4]	3.204E-07	2.470E-06	2.589E-06
J_{xK5} [m4]	-	1.046E-06	-
J_{xK6} [m4]	-	3.937E-07	-
J_{yc} [m4]	6.140E-03	5.059E-03	3.680E-03
A_w [m2]	3.100E-03	8.600E-03	2.990E-03

Symbols: s_c – the cross-beam spacing, m; s_g – the truss girder spacing, m; H_t – the theoretical height of a truss girder, m; L_t – the theoretical length of a truss girder, m.

The analytical method of setting rotational end restraint was applied to all cross-beams of the analyzed bridge spans. The data used for computations are gathered in Table 2.

Fig. 15 Rotational end restraint for cross-beams: the Span-51 (top), the Span-93 (middle), the Span-38 (bottom)

The analysis results are given in Fig. 15. Rotational end restraints r_c for the cross-beams, based on the FEM analysis and the analytical method, are put together in three diagrams – for the Span-51, the Span-93 and the Span-38, respectively.

In general, the results based on the analytical method show good agreement with those obtained from the FEM analysis. The largest discrepancies occur for the support cross-beams of the Span-51 and the Span-93 and for the twin cross-beams of the Span-93. Support diagonals of both spans are connected at their top by a pair of transverse beams (see Fig. 13). In the FE analysis the twin cross-beams of the Span-93 had to be loaded simultaneously by a locomotive boogie. Both circumstances cannot be taken into account in the analytical method. For the other cross-beams of the Span-51 and the Span-93 the result discrepancy was 2÷35%. The smallest discrepancies (0÷2%) occur for the cross-beams of the Span-38, probably because its layout is the most coherent with the analytical model.

It can be seen that the rotational end restraint for the cross-beams of railway through truss bridges varies alongside each bridge span. For the analysed bridge spans the restraint for the cross-beams connected to truss chords between the chord nodes is even two times smaller than the restraint for the cross-beams connected to the chord nodes. In each group values of restraint fall in certain range: 40÷80 MN/rad for the inter-nodal cross-beams and 110÷150 MN/rad for the nodal cross-beams.

The obtained values of rotational end restraint for the cross-beams of railway through truss bridges allow for the creation of a computational model of a cross-beam as a separate member. For the assessment of the bending moment at the cross-beam – to – truss chord connection the following values of rotational end restraint are suggested to be taken as upper limits: 80 MN/rad for the cross-beams connected to truss chords between the chord nodes and 150 MN/rad for the cross-beams connected to the chord nodes. It should be noted that the above suggestion is based on the analysis of truss girders built of open cross-section members.

4. Conclusions

Considering the presented analytical method and the analysis results the following conclusions can be drawn:

1. It is possible to make an analytical approximation of rotational end restraint for cross-beams of railway through truss bridges. It is expected that similar assessment is feasible for other twin girder bridges.

2. The analytical method proves that the rotational end restraint for cross-beams of railway through truss bridges is governed by flexural and torsional stiffness of truss and deck members as well as axial stiffness of wind bracing in the close vicinity of the analysed cross-beam.
3. Wind bracing members situated away from cross-beam neutral axis play important role in restraining cross-beam end rotation. Assuming equal eccentricity in respect to cross-beam neutral axis K-type wind bracing is more efficient than X-type wind bracing.
4. The restraint for the cross-beams connected to truss chords between chord nodes is significantly smaller than the restraint for the cross-beams connected to the chord nodes. In each group of cross-beams values of the restraint are similar.
5. For the assessment of the bending moment at the cross-beam – to – truss chord connection, for the cases similar to the studied ones, the following upper limit values of the rotational end restraint are suggested: 80 MN/rad for the inter-nodal cross-beams (connected to truss chords between chord nodes) and 150 MN/rad for the nodal cross-beams (connected to the chord nodes).
6. Setting the rotational end restraint for a cross-beams according to the presented method, makes it possible to model and analyze the beam as a separate member. Such approach can be applied in preliminary design and rapid assessment of bending moment distribution due to service load.

Acknowledgements

The support of the 503218/01/12/DSPB/0627 and 503217/01/12/DSPB/0590 grants of the Ministry of Science and Higher Education of Republic of Poland is kindly acknowledged.

References

Adman, R. and Saidani, M. (2013) "Elastic buckling of columns with end restraint effects", *J. Constr. Steel Res.*, **87**, 1-5, https://doi.org/10.1016/j.jcsr.2013.03.022

Balázs, I. and Melcher, J. (2017), "Influence of uplift load on torsional restraint provided to steel thin-walled purlins by sandwich panels", *Procedia Eng.*, **190**, 35-42, https://doi.org/10.1016/j.proeng.2017.05.304

Balázs, I., Melcher, J. and Belica, A. (2016), "Experimental investigation of torsional restraint provided to thinwalled purlins by sandwich panels under uplift load", *Procedia Eng.*, **161**, 818-824, https://doi.org/10.1016/j.proeng.2016.08.718

Blum, H.B. and Rasmussen, K.J.R. (2018), "Elastic buckling of columns with a discrete elastic torsional restraint", *Thin-Wall. Struct.*, **129**, 502-511, https://doi.org/10.1016/j.tws.2018.01.008

Caglayan, O., Ozakgul, K. and Tezer, O. (2012), "Assessment of existing steel railway bridges", *J. Constr. Steel Res.*, **69**, 54-63, https://doi.org/10.1016/j.jcsr.2011.08.001

Cavadas, F., Rodrigues, C., Félix, C. and Figueiras, J. (2013), "Post-rehabilitation assessment of a centenary steel bridge through numerical and experimental analysis", *J. Constr. Steel Res.*, **80**, 264-277, https://doi.org/10.1016/j.jcsr.2012.09.020

Durif, S., Bouchaïr, A. and Bacconnet, C. (2015), "Elastic rotational restraint of web-post in cellular beams with sinusoidal openings", *Steel Compos. Struct.*, **18**(2), 325-344; http://dx.doi.org/10.12989/scs.2015.18.2.325

Gajdzicki, M. (2018), "Sheet-to-purlin fasteners arrangement and the value of rotational restraint of cold-formed Z-purlins", *J. Constr. Steel Res.*, **151**, 185-193, https://doi.org/10.1016/j.jcsr.2018.09.028

Gao, T. and Moen, C.D. (2012), "Predicting rotational restraint provided to wall girts and roof purlins by through-fastened metal panels", *Thin-Wall. Struct.*, **61**, 145-153, https://doi.org/10.1016/j.tws.2012.06.005

Lim, N.S., Tan, K.H. and Lee, C.K. (2017), "Effects of rotational capacity and horizontal restraint on development of catenary action in 2-D RC frames", *Eng. Struct.*, **153**, 613-627, https://doi.org/10.1016/j.engstruct.2017.09.059

Lu, Y., Cheng, Y. and Han, Q. (2017), "Experimental investigation into the in-plane buckling and ultimate resistance of circular steel arches with elastic horizontal and rotational end restraints", *Thin-Wall. Struct.*, **118**, 164-180, https://doi.org/10.1016/j.tws.2017.05.010

Marsh, K. (2016), "Autodesk Robot Structural Analysis Professional 2016: essentials", Marsh API

Nguyena, P.C. and Kim, S.E. (2017), "Investigating effects of various base restraints on the nonlinear inelastic static and seismic responses of steel frames", *Int. J. Non-linear Mech.*, **89**, 151-167, https://doi.org/10.1016/j.ijnonlinmec.2016.12.011

Pi, Y.L. and Bradford, M.A. (2013a), "Lateral–torsional elastic buckling of rotationally restrained arches with a thin-walled section under a central concentrated load", *Thin-Wall. Struct.*, **73**, 18-26, https://doi.org/10.1016/j.tws.2013.07.006

Pi, Y.L. and Bradford, M.A. (2013b), "In-plane stability of preloaded shallow arches against dynamic snap-through accounting for rotational end restraints", *Eng. Struct.*, **56**, 1496-1510, https://doi.org/10.1016/j.engstruct.2013.07.020

Pi, Y.L. and Bradford, M.A. (2013c), "Nonlinear analysis and buckling of shallow arches with unequal rotational end restraints", *Eng. Struct.*, **46**, 615-630, https://doi.org/10.1016/j.engstruct.2012.08.008

Vičan, J., Jošt, J. and Gocál, J. (2014), "Analysis of the stringer-to-cross-beam riveted joint behaviour", *Civil Environ. Eng.*, **10**(1), 50-60, https://doi.org/10.2478/cee-2014-0007

Wang, R., Huang, Y., Li, Q. and Zhen, X. (2009), "Model test and numerical analysis of a special joint for a truss bridge", *J. Constr. Steel Res.*, **65**, 1261-1268, https://doi.org/10.1016/j.jcsr.2009.02.002

Wu, B. and Zhang, R. (2017), "Rotational restraint stiffness of concrete beam-slab assembly exposed to fire", *Procedia Eng.*, **210**, 479-487, https://doi.org/10.1016/j.proeng.2017.11.104

Zhou, W. and Jiang, L. (2016), "Distortional buckling of cold-formed lipped channel columns subjected to axial compression", *Steel Compos. Struct.*, **23**, 331-338, https://doi.org/10.12989/scs.2017.23.3.331

Zhou, W., Li, S., Huang, Z. and Jiang, L. (2016), "Distortional buckling of I-steel concrete composite beams in negative moment area", *Steel Compos. Struct.*, **20**(1), 57-70, https://doi.org/10.12989/scs.2016.20.1.057

Zhou, W., Li, S., Jiang, L. and Huang, Z. (2015), "Distortional buckling calculation method of steel-concrete composite box beam in negative moment area", *Steel Compos. Struct.*, **19**(5), 1203-1219, https://doi.org/10.12989/scs.2015.19.5.1203

CC